Digital imaging of clear-sky polarization

Raymond L. Lee, Jr.

If digital images of clear daytime or twilight skies are acquired through a linear polarizing filter, they can be combined to produce high-resolution maps of skylight polarization. Here polarization P and normalized Stokes parameter Q are measured near sunset at one inland and two coastal sites. Maps that include the principal plane consistently show that the familiar Arago and Babinet neutral points are part of broader areas in which skylight polarization is often indistinguishably different from zero. A simple multiple-scattering model helps explain some of these polarization patterns.

OCIS codes: 260.5430, 010.1290, 290.4210, 100.2000.

1. Introduction

Observations of clear-sky polarization have a venerable history that includes such 19th century icons of optics as David Brewster (1781–1868), Jacques Babinet (1793–1872), and François Arago (1786–1853).[1] In his pivotal 1871 paper on sky color and polarization, Lord Rayleigh (1842–1919) provided a succinct theoretical explanation for skylight's maximum polarization 90° from the Sun. Rayleigh did not mention the neutral points (points of zero polarization) observed in the Sun-zenith plane by Arago, Babinet, and Brewster. Although Rayleigh was confident that he had "disposed of the polarization" problem,[2] others did not view his silence on the neutral points as a proscription.[3]

In fact, the extensive literature on clear-sky polarization left by Rayleigh's contemporaries has been greatly expanded in 20th century studies by (among others) Dorno, Jensen,[4] Neuberger,[5] Sekera,[6] Coulson,[7] and Volz.[8] Many of these studies' measurements have been made with naked-eye polarimeters either held by hand or mounted on a clinometer.[8,9] Yet even electronic polarimeters usually yield only spot observations of polarization averaged over their narrow fields of view (FOV). This restriction has tended to limit the angular extent of polarization studies, which often are confined to the Sun-zenith (or principal) plane or to the zenith itself.[7,10]

Thus, in the past, skylight polarization was analyzed outside the principal plane only occasionally.[11,12] Yet now we can routinely measure polarization almost anywhere in the sky hemisphere by using digital imaging techniques—in my case, digitized color slides. Because skylight is mostly linearly (rather than circularly) polarized,[13–15] I can use a dichroic linear polarizing filter as an analyzer. The resulting maps of polarized sky radiances can be (1) acquired as quickly as photographs can be taken, and (2) readily manipulated to produce maps of skylight polarization. In addition to their flexibility, digital-image polarization data have unprecedented angular detail and extent. The high spatial and temporal resolution of these maps can improve skylight polarization models as well as the physical insights that underlie them.

2. Measuring Skylight's Degree of Linear Polarization

Compared with such seemingly straightforward quantities as skylight's radiance and chromaticity, measures of its polarization may appear obscure to newcomers. Graphs of polarization ratio versus scattering angle[16] and hemispheric maps of Stokes parameters and of (partial) polarization planes[17] can at first seem far removed from simple observations of skylight through a polarizer. Of course, historically, skylight polarization was first quantified by such simple means. To identify skylight's neutral points, observers such as Brewster and Arago needed only to interpret visually the images that they saw through a polarimeter (e.g., the description of the Savart polariscope's use in Ref. 5).[18]

To quantify polarization further, we now use Stokes parameters to define various measurable degrees of polarization. For Stokes parameters I, Q,

The author is with the Department of Oceanography, U.S. Naval Academy, Annapolis, Maryland 21402.

Received 22 May 1997; revised manuscript received 11 August 1997.

0003-6935/98/091465-12$15.00/0

U, and V, the total degree of polarization P_T is given by[19]

$$P_T = \frac{(Q^2 + U^2 + V^2)^{1/2}}{I}, \tag{1}$$

where I is the scattered irradiance and Q, U, and V are irradiances related to the scattered light's ellipsometric parameters.[20] By choosing a linear polarizer as my analyzer, I can measure only skylight's degree of linear polarization P, where

$$P = \frac{(Q^2 + U^2)^{1/2}}{I}, \tag{2}$$

thus ignoring skylight's minimal degree of circular polarization, V/I.[21]

Although we can use digital-image radiances rather than irradiances in Eq. (2), this still leaves the practical problem of defining the Stokes parameters in terms of those radiances. For measurements of P, Fitch *et al*. define convenient relationships between I, Q, and U and digital-image radiances.[22] In their work, they made four digital images of a scene with a linear polarizer rotated to four different relative positions: 0°, 45°, 90°, and 135°. The 0° direction can be arbitrary if we do not need to know the azimuth χ of the vibration ellipse for skylight's polarized component.[23] For linearly polarized light, the vibration ellipses are in fact lines. Note that ellipsometric azimuths χ are different from ϕ_{rel}, azimuth relative to the Sun (see below).[24]

At corresponding pixels in a scene's four digital images, the relative radiances $L(0°)$, $L(45°)$, $L(90°)$, and $L(135°)$ are related to the Stokes parameters by

$$\begin{aligned} I &= 0.5[L(0°) + L(45°) + L(90°) + L(135°)], \\ Q &= L(0°) - L(90°), \\ U &= L(45°) - L(135°). \end{aligned} \tag{3}$$

Results from Eqs. (3) are used in Eq. (2) to calculate linear polarization P. Equations (3)'s four-image technique is indispensable if a lens' FOV is quite large, such as for a fish-eye lens. Yet for the much smaller FOV of a normal 35-mm camera lens ($\sim 37° \times 25°$), even two images can provide useful, although incomplete, information about clear-sky polarization. Furthermore, the completeness of Eqs. (3) comes at the cost of extra image processing and added uncertainties in geometrically registering four, rather than two, images. As a final caution, note that skylight polarization has been measured with any number of polarizer directions,[25] and each of these techniques will produce similar (but not likely identical) P values. Every additional polarizer direction increases the information available for calculating P at each pixel and, in principle, improves the accuracy of P.

What can be learned from the simpler, although more limited, two-image technique? First, two-image measurements have historical significance; in the past, zero Q was often equated with neutral P.[4,26] Thus seeing the relationship between Q and P provides insights into earlier research. Second, Stokes parameters Q and U are useful by themselves in quantifying skylight polarization, and either can be determined from pairs of polarized digital images.

Suppose that we (1) include the principal plane[27] ($\phi_{\text{rel}} = 0°$ or 180°) in the FOV of a camera equipped with a normal lens and (2) rotate a linear polarizer mounted on that lens so that its transmission axis is horizontal. Above the Arago neutral point, χ is also horizontal, and so the angle between χ and the transmission axis is 0° there (χ is vertical below the Arago point). Call radiances measured at this filter orientation $L(0°)$. Rotating the filter 90° makes its transmission axis vertical and yields $L(90°)$. Given that $U = Q \tan(2\chi)$ and, in principle, χ forms angles of 0° or 90° with the principal plane, then $U = 0$ for all skylight observations there.[28] Now define the Q-component contribution to polarization as p_Q, where

$$p_Q = \frac{L(0°) - L(90°)}{L(0°) + L(90°)}, \tag{4}$$

with 90° and 0° measured relative to χ. p_Q can also be regarded as a normalized Stokes parameter Q, although without Q's additive properties for different scattering mechanisms. Naturally, Eq. (4) offers the advantage of requiring only two polarized digital images rather than Eqs. (3)'s four.

Assuming $U = 0$ in the principal plane, then p_Q is the signed equivalent of Eq. (2)'s P [except for small differences in the denominators of Eqs. (2) and (4)]. At the single-scattering level, Eq. (4)'s directions are measured with respect to the scattering plane. For single scattering by spheres, Eq. (4) in fact defines the signed polarization.[29] $P \neq |p_Q|$ wherever U is nonzero, although P and p_Q may actually differ very little. In the principal plane, p_Q and P are nearly identical.

Outside the principal plane, linear polarization P still can be determined unequivocally from two filter directions if the detector has a very narrow FOV (say, $\ll 1°$). Rotate the polarizing filter to obtain the FOV's radiance extremes $L_{\max}$ and $L_{\min}$ and then calculate P as[30]

$$P = \frac{L_{\max} - L_{\min}}{L_{\max} + L_{\min}}. \tag{5}$$

Note that Eqs. (2) and (5) both determine the same linear P, although they use different measurement techniques. For linearly polarized skylight, $L_{\max}$ and $L_{\min}$ will occur at filter directions 90° apart. Once again, extrapolate this to a camera equipped with a normal FOV lens and polarizing filter. Although the camera lens has a FOV $\gg 1°$, individual pixels within that FOV receive radiances from very small solid angles ($< 1 \times 10^{-6}$ sr). Aim the camera at some arbitrary point in the clear sky and rotate the polarizer to obtain the brightest image as measured by the camera's light meter. Call this the $L_{\max}$ im-

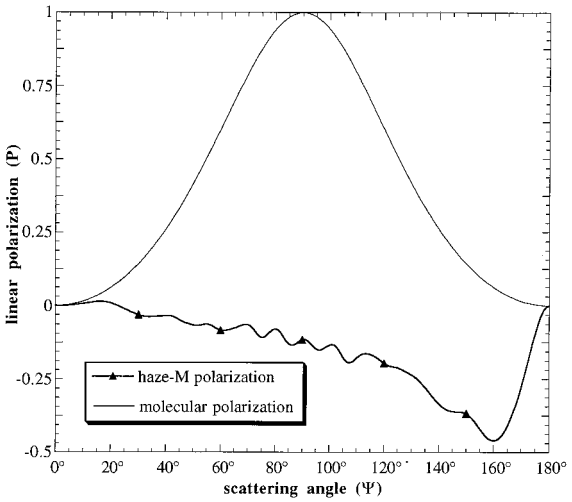

Fig. 1. Signed polarization as a function of scattering angle Ψ for scattering by a small sphere (approximately molecular scattering) and by an ensemble of spherical haze droplets whose size spectrum follows the Deirmendjian haze-M distribution at $\lambda = 475$ nm. The haze droplets' real and imaginary refractive indices are 1.5 and 0.01, respectively.

age; rotating the polarizer by 90° yields the $L_{\min}$ image.

Many pixels in the $L_{\max}$ and the $L_{\min}$ images approximately meet Eq. (5)'s conditions for calculating P. Because there are only two fixed polarizer directions and χ varies across the lens' FOV, many pixels would require a slightly different pair of polarizer directions for calculating their true P. In fact, because $U \neq 0$ outside the principal plane, we are actually calculating p_Q for most pixels. Yet wherever (1) polarization is strong and (2) Eq. (4)'s 0° direction corresponds to χ, then $p_Q \sim P$ because conditions (1) and (2) require that $|U| \ll |Q|$. Furthermore, I have independently confirmed that $p_Q \sim P$ when P is large. I did this by comparing maps of two-image p_Q and four-image P in the same clear sky at 90° from the Sun. In this strongly polarized sky, patterns of p_Q and P are virtually the same and χ changes less than 4° across my normal lens' FOV. However, when χ changes, so will Eq. (4)'s p_Q values, an issue addressed below. Not surprisingly, the combination of variable χ and two fixed polarizer directions can generate negative p_Q, even outside the principal plane.

Some changes in χ (and thus p_Q's sign) can be explained by haze scattering. Figure 1's top curve shows polarization as a function of scattering angle Ψ for an isotropic molecule. Here polarization is always nonnegative, and Rayleigh's theory predicts complete polarization at $\Psi = 90°$. In fact, molecular anisotropy reduces the maximum single-scattering molecular P to ~0.92–0.94.[31] Figure 1's bottom curve shows the usually negative polarization that results from scattering by the Deirmendjian haze-M droplet-size spectrum at wavelength $\lambda = 475$ nm.[32] When polarization by the haze drop-size distribution is equivalent to that by some mean-sized droplet, then Fig. 1 also gives haze's single-scattering contribution to p_Q. In a multiple-scattering atmosphere, the relative contributions of molecules and haze to the observed polarization will be complicated functions of their respective slant optical thicknesses and Ψ. Yet wherever haze scattering predominates that by molecules, p_Q will be negative.

So in general $|p_Q| \neq P$, especially if Eq. (4)'s 0° direction is chosen arbitrarily. This inequality makes sense because the two-image p_Q [Eq. (4)] is based on half as much information as the four-image P [Eq. (2)]. Yet, as shown above, P can be measured unambiguously from only two radiances [Eq. (5)], provided that the detector's FOV is quite small. Although a camera with a normal lens and polarizer takes in a larger FOV, individual pixels within that FOV still approximately meet Eq. (5)'s criteria of maximum and minimum radiance. Furthermore, if we (1) align Eq. (4)'s 0° direction with χ and (2) measure p_Q in the principal plane or in regions of strong polarization, then P and p_Q will be nearly the same because U is negligibly small.

3. Polarizer Performance and Possible Error Sources

A prerequisite for measuring P and p_Q is accurate clear-sky radiances. My sources for these are color slides of clear skies photographed at several sites and times of day. For each scene, I take multiple slides with a 35-mm camera that is mounted on a tripod and equipped with a normal lens and linear polarizing filter. The filter is rotated to yield the various polarized radiances on the right-hand sides of Eqs. (3) and (4). The slides are digitized at a color resolution of 24 bits per pixel, and algorithms developed earlier[33] are used to calibrate the digital images colorimetrically and radiometrically. These images yield relative radiances whose angular resolution is limited only by the film; a resolution of 1/65° is possible.

Although the camera's FOV is fixed in each scene, the polarized images still must be geometrically registered after digitizing. After registration, residual errors vary slowly across the digital images, but typically they are 1:600 pixels or ~0.07° for the two-image technique [Eq. (4)] and approximately twice that for the four-image technique [Eqs. (3)]. Then p_Q or P are calculated pixel by pixel from the entire set of digitized color slides.[34] At each pixel, values are either plotted as a gray-scale pixel or stored for later quantitative analysis. Note that (1) all my radiance and polarization measurements are integrated across the visible spectrum (400–700 nm), and (2) the spectral transmittance T of my polarizing filter is nearly constant ($T \sim 0.32$) at visible wavelengths. Solar glare complicates making accurate polarization measurements, so my polarization maps exclude the Sun. I begin with two-image measurements of skylight's p_Q.

In taking the photographs that produce Fig. 2(a), I oriented the polarizing filter's transmission axis parallel [$L(90°)$] and perpendicular [$L(0°)$] to the vertical principal plane. In Fig. 2(a), this plane's projection is a vertical passing through $\phi_{\text{rel}} = 180°$. Below the Arago point at $\phi_{\text{rel}} = 180°$, the principal plane and χ

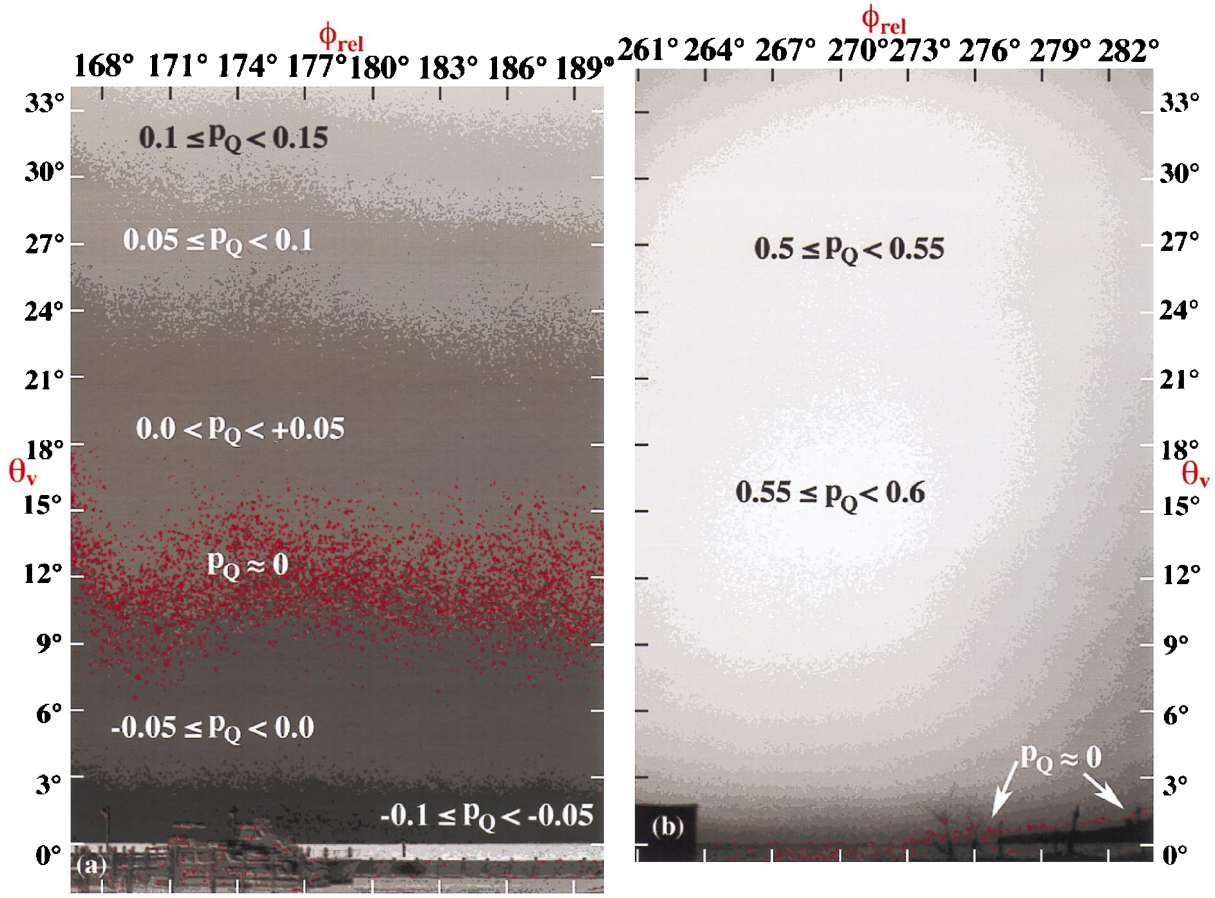

Fig. 2. Maps of clear-sky p_Q at the coastal site of Chesapeake Beach, Md., on 6 February 1996. In map (a), the Sun elevation = 1.8° at 2220 UTC and azimuth relative to the Sun ϕ_{rel} = 180° at map center. In map (b), the Sun elevation = −0.46° at 2234 UTC and the p_Q maximum occurs at ϕ_{rel} = 270°. Each map's angular size is ~23.5° × 36°, and every map gray level spans Δp_Q = 0.05; pixels with $|p_Q| < 0.002$ are colored red.

coincide. For skylight largely due to molecular scattering, χ rotates at most by ~5° at a given view-elevation angle θ_v in Fig. 2(a).[35] Thus the magnitude of p_Q at ϕ_{rel} other than 180° will be reduced simply because the polarizer is slightly misaligned with χ. By how much does this misalignment reduce p_Q?

The short answer is "some in principle, but almost none in practice." To quantify this answer, I first determine my polarizer's optical performance. In polarizer parlance, the extinction coefficient H_{90} is the combined transmittance of initially unpolarized light by two linear polarizers whose transmission axes are crossed at right angles. The photographic polarizer used here has an average visible wavelength $H_{90} = 6.341 \times 10^{-4}$, and its major and minor principal transmittances k_1 and k_2 are 0.6423 and 9.873×10^{-4}, respectively.[36] Given these data, Mueller matrix calculations[37] show that my polarizer can transform unpolarized light into linearly polarized light whose $P = 0.9969$. Call this polarization that is due to the filter itself its intrinsic polarization. Because of the clear-sky maximum of $P \sim 0.85$, my filter's performance is entirely adequate for measuring skylight polarization. The same polarizing filter is used for all measurements, including those of Figs. 2–4.

Now we can answer the question posed above: how does polarizer alignment affect skylight p_Q?[38] Figure 5 shows Mueller matrix calculations based on my filter's intrinsic polarization and on the angle ϑ between its transmission axis and χ. These calculations yield Eq. (5)'s degree of polarization for completely linearly polarized light ($P = 1$) observed through my polarizer when it is misaligned ϑ degrees with respect to χ. This underestimation of the light source's true polarization is a depolarization that is caused both by the polarizer's intrinsic polarization ($P = 0.9969$) and by its rotation. Call this underestimation $d(\vartheta)$.

As a multiplicative factor, $d(\vartheta)$ can be used to correct polarization underestimations, provided that we know χ's orientation. In principle, that orientation is either vertical or horizontal at ϕ_{rel} = 180° and 0°. In Figs. 2 and 3 my threshold for neutral p_Q is 0.002, and I have colored pixels red in which $|p_Q| < 0.002$. Now suppose that $L(0°)$ were measured with the polarizer's transmission axis rotated 5° from χ. Then the observed threshold p_Q is actually $0.002/d(5°)$, or 0.002037—a negligibly small error. In other words,

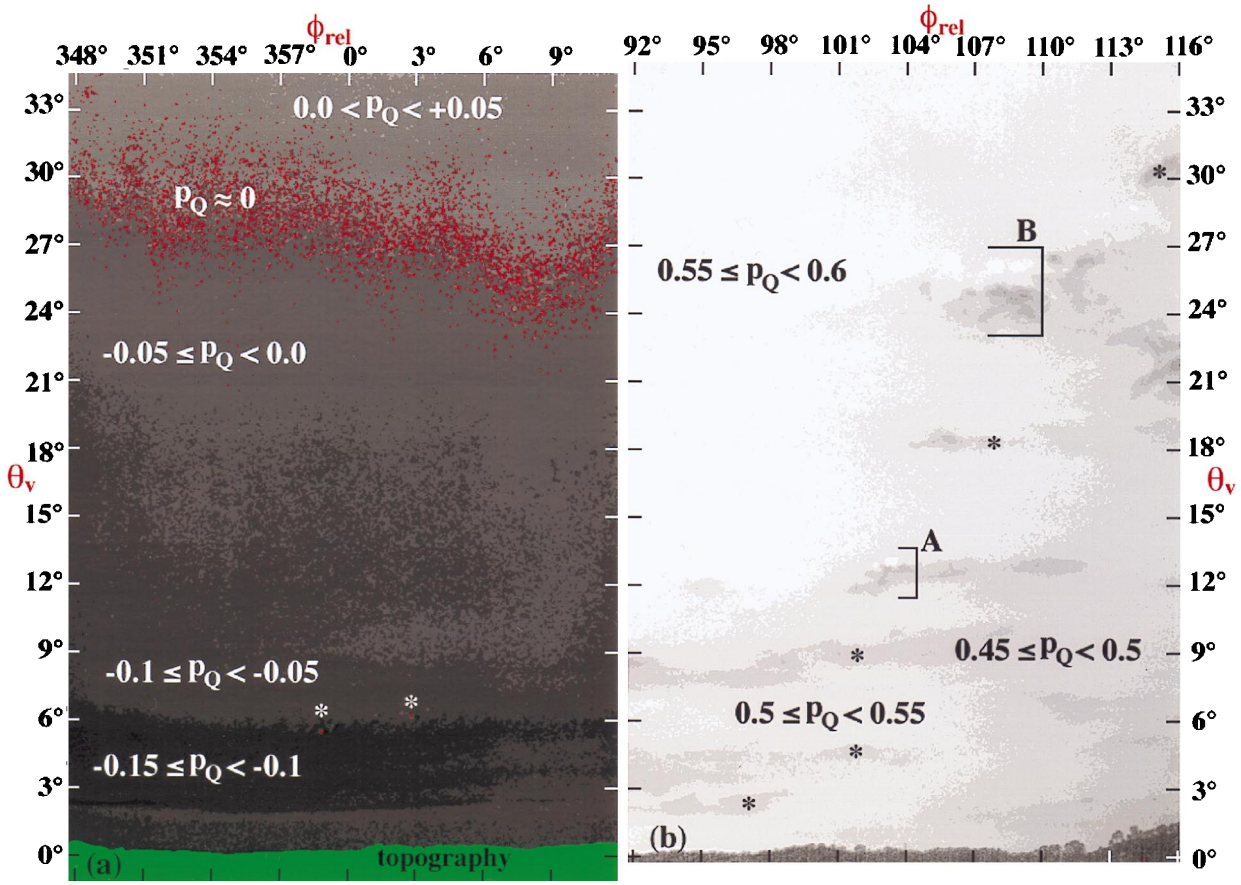

Fig. 3. Maps of clear-sky polarization p_Q at Marion Center, Pa., on 31 August 1996. This inland site is ~425 km from the Atlantic Ocean, and its elevation is 450 m above mean sea level. In map (a), the Sun elevation = −0.7° at 2352 UTC and the center $\phi_{rel} = 0°$; in map (b), the Sun elevation = 8.7° at 2259 UTC and the center $\phi_{rel} = 104°$. Each map's angular size is ~24.3° × 35.7°.

because $d(\vartheta)$ is a multiplier, its greatest arithmetic effects are on large p_Q values, and at most these will be only ~1.9% if $\vartheta \leq 5°$. Thus $d(\vartheta)$ does not significantly increase or decrease the number of near-neutral red pixels in Fig. 2(a). Counterbalancing (and perhaps outweighing) this small depolarization is the camera optics' self-polarization due to refraction.[39]

Other possible error sources are likely to be self-correcting. Consider (1) geometric exposure falloff on the film plane (e.g., vignetting) and (2) the fact that rays with different incidence angles follow differently slanted optical paths through the filter's dichroic layer. In principle, both factors produce radial radiance patterns in the digital images. However, because the exposure reductions are the same fraction of the film-plane radiances for all filter orientations, their effects in Eqs. (2) and (4) should be self-canceling. In any event, Figs. 2–4 do not show any consistent radial patterns of polarization or depolarization.

4. Two-Image Analyses of Clear-Sky Polarization: A Coastal Site

In Fig. 2(a), we look ENE over Maryland's Chesapeake Bay just before sunset on 6 February 1996. This figure is a gray-scale map of p_Q as measured by Eq. (4)'s two-image technique (map time and place are further specified below). At Fig. 2(a)'s center, $\phi_{rel} = 180°$, so there we are looking in the principal plane where $p_Q = P$ (assuming $U = 0$ there). Figure 2(b) shows p_Q a few minutes later at the same site. Now $\phi_{rel} \sim 270°$ at image center, and the compass direction there is SSE. Each map's angular dimensions in Fig. 2 are ~23.5° × 36°. Throughout Figs. 2–4, each gray level spans $\Delta p_Q = 0.05$, and representative p_Q values are labeled on the maps.

As expected, polarization is near zero some distance above the antisolar horizon. Figure 2(a)'s red pixels ($|p_Q| < 0.002$) vividly illustrate that the Arago point has many neutral and near-neutral neighbors both in and immediately outside the principal plane. (Recall that p_Q is only the Q-component contribution to total polarization.) In fact, neutral bands such as that in Fig. 2(a) have been observed before. Dorno's 1917 observations of skylight polarization at Davos, Switzerland, included what he termed "neutral lines," which, properly speaking, are only lines of Q (or p_Q) = 0.[4,40] As Coulson notes, "the term neutral line is somewhat misleading, as $P \neq 0$ at neutral lines except as they intersect the Sun's vertical at the neutral points, where indeed $P = 0$."[28]

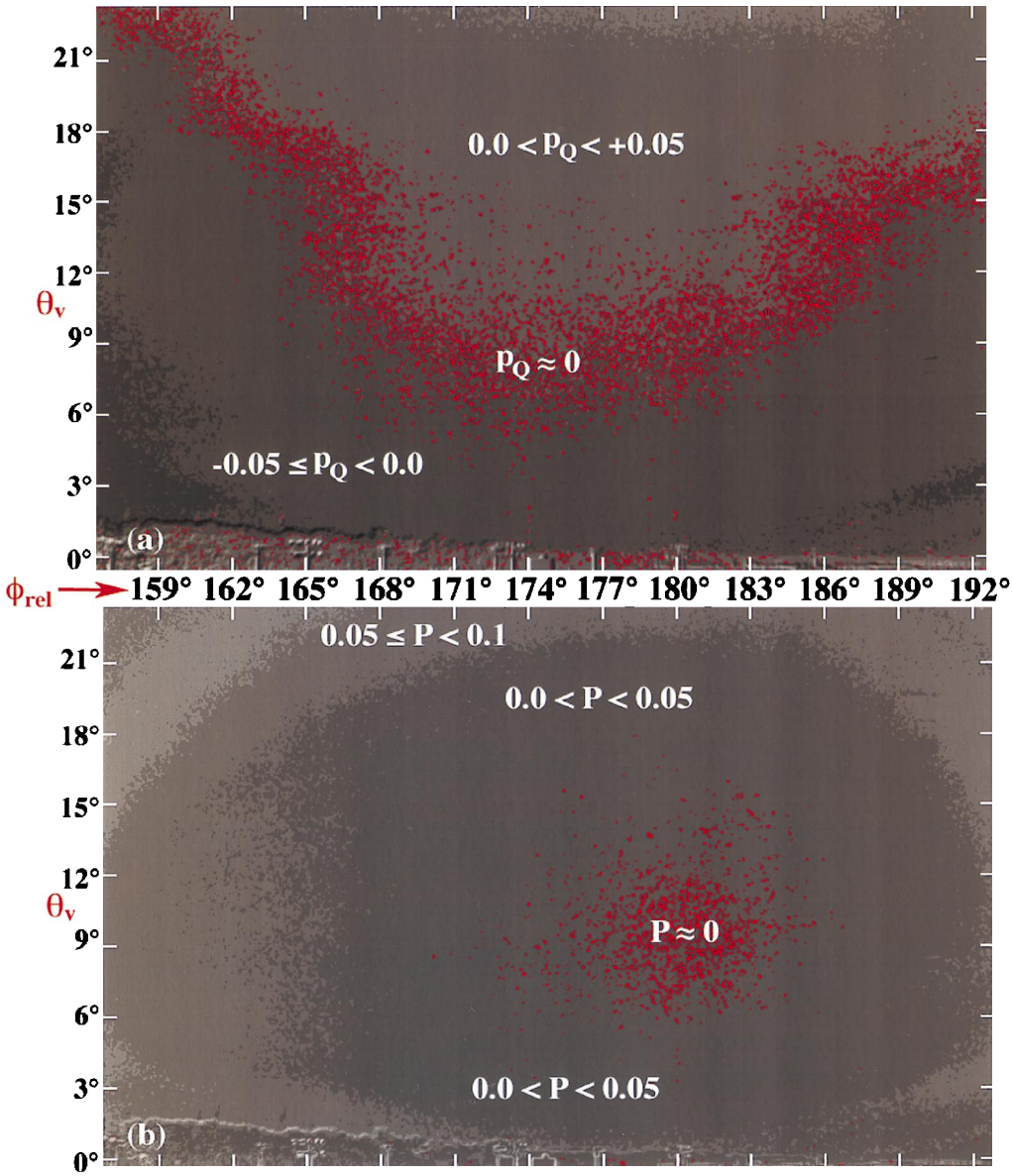

Fig. 4. Comparison of p_Q [map (a)] and P [map (b)] for the antisolar clear sky at Annapolis, Md., on 12 March 1997 at 2255 UTC. In both maps, $\phi_{rel} = 180°$ is marked and the Sun elevation = 2.4°. In map (a), pixels are colored red for $|p_Q| < 0.002$; in map (b) the criterion is $P < 0.005$. Each map's angular size is ~36.2° × 23.8°.

Figure 6 shows a meridional profile of p_Q ($\approx P$) in Fig. 2(a)'s principal plane. An Arago point occurs at $\theta_v = 11.7°$ in Fig. 6, some 13.5° above the antisolar point. Pixels are averaged 2° on either side of the principal plane in calculating Fig. 6's observed p_Q, and its error bars are based on standard deviations of Fig. 7's radiances within the 4° azimuthal swath. Figure 6's low Arago distances have been observed before over water, although usually for higher Sun elevations.[41] The boundary between negative and positive polarization at the horizon is both easy to see and understand here. Skylight reflected from the Chesapeake Bay's planar surface toward the camera will have positive polarization for many different incidence angles (here a typical water $P \sim 0.15$).[42]

Figure 2(b)'s p_Q maximum of ~0.57 occurs near image center at $\phi_{rel} = 270°$. If scattering were exactly symmetric about the principal plane, this map would be identical to one for $\phi_{rel} = 90°$. However, the irregular p_Q patterns around $\phi_{rel} = 180°$ and 0° in Figs. 2(a) and 3(a) show that such polarization symmetry is not guaranteed. In Fig. 2(b), the 0° filter direction was the one that gave the brightest image as measured by the camera's light meter. In this $L(0°)$ image, the filter's transmission axis was rotated ~22° clockwise from the vertical, as Fig. 2(b)'s tilted axis of maximum p_Q suggests. That my choice of $L(0°)$ and $L(90°)$ produced large p_Q also suggests that $p_Q \sim P$ here. Further evidence that $p_Q \sim P$ in this strongly polarized region comes from Fig. 2(b)'s resemblance to Bullrich's maps of polarization maxima observed well outside the principal plane: Fig. 2(b)'s maximum is at

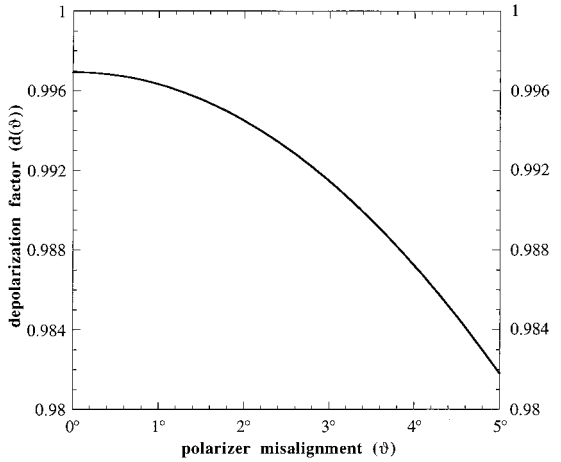

Fig. 5. Depolarization factor d(ϑ) as a function of the misalignment ϑ of my polarizing filter's transmission axis relative to χ. If a light source were completely linearly polarized, these d(ϑ) would equal its P [Eq. (5)] as measured for polarizer misalignments of $0° \le \vartheta \le 5°$.

$\theta_v \sim 14.6°$.[12] p_Q decreases near Fig. 2(b)'s sides, as expected when Ψ approaches 180° and 0°. In the haze layer just above the horizon, p_Q is occasionally negative, perhaps because negatively polarized scattering by haze droplets dominates there (see Fig. 1 for $70° < \Psi < 170°$). Also evident near Fig. 2(b)'s horizon is a steep p_Q gradient, a feature caused by the rapid increase of optical thickness with zenith angle. The enhanced multiple scattering that results will rapidly depolarize near-horizon skylight even though p_Q is large at higher θ_v. Earlier research had hinted at such polarization gradients near the horizon,[43] but digital imaging reveals them in unprecedented detail.

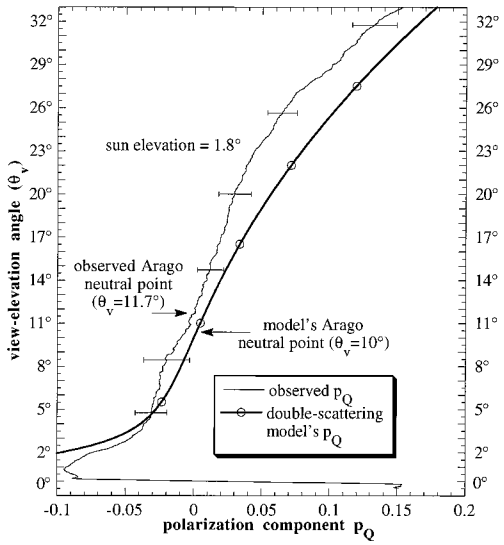

Fig. 6. Clear-sky polarization component p_Q ($\approx P$ here) at Chesapeake Beach, Md., on 6 February 1996 at 2220 UTC for $\phi_{rel} = 180°$ [see Fig. 2(a)]. Each error bar spans two standard deviations of p_Q at the given θ_v and is calculated from the standard deviations of Fig. 7's radiances. The above-horizon rms difference between observed polarizations and those predicted by a double-scattering model = 0.0359. The model wavelength is 475 nm, and its molecular and aerosol normal optical depths are 0.15 and 0.05, respectively.

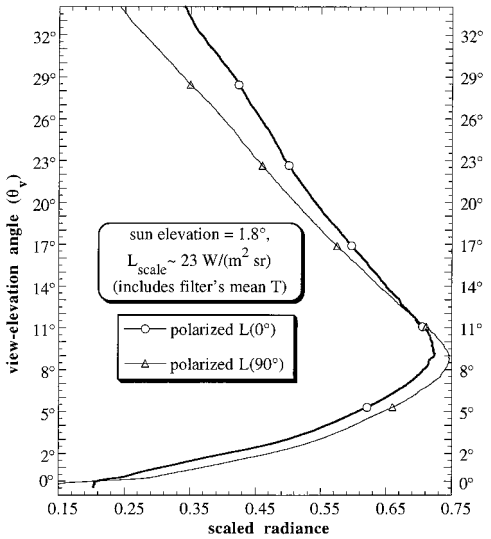

Fig. 7. Polarized clear-sky radiances looking ENE over the Chesapeake Bay (Chesapeake Beach, Md.) on 6 February 1996 at 2220 UTC. The Sun's elevation = 1.8°, and the measurement meridian's azimuth relative to it (ϕ_{rel}) is 180°. Radiances were averaged 2° on either side of the principal plane, and the $L(0°)$ were measured with the polarizing filter's transmission axis perpendicular to that plane (i.e., oriented horizontal). Multiplying the scaled radiances by L_{scale} approximates the absolute radiances at the film plane, including the effects of the filter's average spectral transmittance T.

Figure 8 shows meridional radiance profiles of $L(0°)$ and $L(90°)$ averaged over a 4°-wide swath that spans Fig. 2(b)'s polarization maximum. Except at small θ_v, Fig. 8's $L(0°)$ and $L(90°)$ differ much more

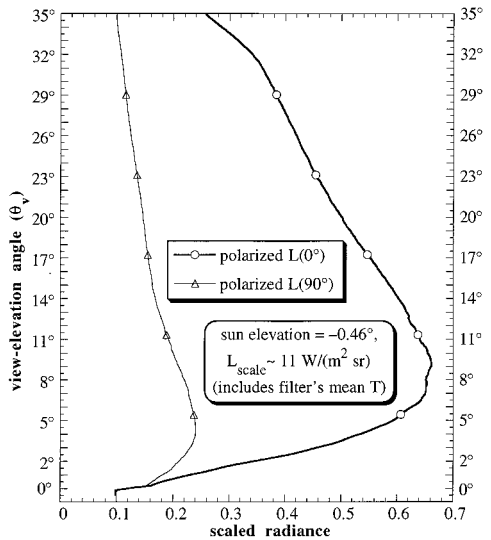

Fig. 8. Polarized clear-sky radiances looking SSE at Chesapeake Beach, Md., on 6 February 1996 at 2234 UTC. The Sun elevation = −0.46°, and $\phi_{rel} = 270°$. Radiances were averaged 2° on either side of $\phi_{rel} = 270°$, and the $L(0°)$ were measured at the filter orientation that produced the brightest image of this scene.

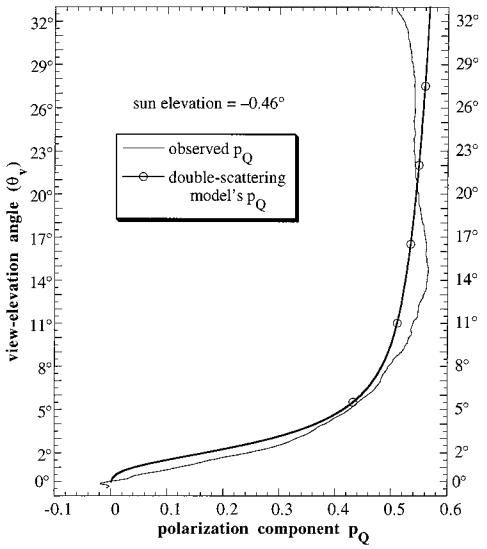

Fig. 9. Clear-sky p_Q ($\sim P$) at Chesapeake Beach, Md., on 6 February 1996 at 2234 UTC for $\phi_{rel} = 270°$ [see Fig. 2(b)]. The above-horizon rms difference between observed polarizations and those predicted by a double-scattering model = 0.0309. The model wavelength is 475 nm, and its molecular and aerosol normal optical depths are 0.15 and 0.05, respectively.

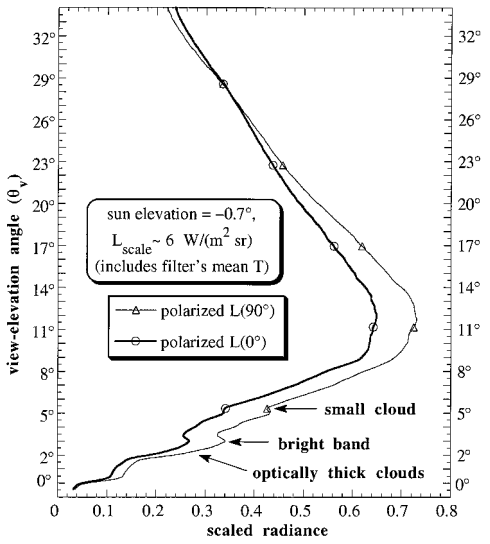

Fig. 10. Polarized clear-sky radiances in the sunset sky near Marion Center, Pa., on 31 August 1996 at 2352 UTC. The Sun elevation = −0.7°, and $\phi_{rel} = 0°$. Radiances were averaged 2.5° on either side of the principal plane, and the $L(0°)$ were measured with the polarizing filter's transmission axis perpendicular to that plane (i.e., oriented horizontally).

than they do in Fig. 7. Naturally, that large difference appears as consistently large values in Fig. 9's meridional profile of p_Q ($\sim P$). Figure 9 also shows a rapid decrease in p_Q above $\theta_v = 32°$, and Fig. 2(b) confirms that this trend occurs at all ϕ_{rel} in the image. Bullrich also observed such sharply defined polarization maxima.[12]

5. Two-Image Analyses of Clear-Sky Polarization: An Inland Site

Figure 3(a) maps p_Q in a mostly clear sunset sky near Marion Center, Pa., on 31 August 1996. Similar to those of Fig. 2, the angular dimensions of Figs. 3(a) and 3(b) are each ~24.3° × 35.7°. In Fig. 3(a) optically thin clouds cover the sky within 9.5° of the topographic horizon (land is colored green), becoming optically thick only at $\theta_v < 2.2°$. The most negative p_Q are concentrated not in the optically thick clouds at the horizon but in the thinner clouds above (note that the darkest band is slightly above the horizon). Scattering geometry and optical thicknesses are much different than in Fig. 2(b), yet once again greater optical thickness is associated with smaller (absolute) p_Q. In fact, a small optically thick cloud atop Fig. 3(a)'s most negatively polarized region has some positive polarization (see points just below the asterisks). Recall that map pixels are colored red when $|p_Q| < 0.002$. Isolated red pixels within the small cloud show just how great its range of p_Q is, as it is embedded in a region where $|p_Q| > 0.05$.

A neutral band is evident at Fig. 3(a)'s top, as is that band's asymmetry about the principal plane. A Babinet neutral point exists at $\phi_{rel} = 0°$ within the neutral band indicated by the red dots, yet dismissing all of its red neighbors as spurious seems unwarranted. Although polarization models may define neutral *points* in hypothetical clear skies, in real clear skies, p_Q observations at best show only neutral and near-neutral *areas*. As Fig. 4(b) indicates, even a four-image polarization map does not reduce the Arago area to a point, nor will allowing red pixels only when $p_Q \equiv 0.0$. For all practical purposes, measurements can never tell us when $p_Q \equiv 0.0$,[44] and thus we can never insist that we have found *the* Babinet (or Arago) neutral point for a given clear sky.

Figure 10 compares the polarized radiance profiles at Marion Center, Pa., for $\phi_{rel} = 0°$. As in Fig. 8, Fig. 10's $L(0°)$ were measured with the polarizer transmission axis horizontal. Here $L(90°)$ exceeds $L(0°)$ at most θ_v, making p_Q negative. The $L(0°)$ and the $L(90°)$ curves cross at $\theta_v = 28°$, the elevation angle of a Babinet neutral point. Because Fig. 3(a)'s optically thick small cloud is silhouetted against the bright twilight sky, it appears as a local minimum in the radiance profiles at $\theta_v = 5.2°$. Yet the strong small-scale depolarization that this cloud exhibits in Fig. 3(a) is not evident in Fig. 11 because p_Q's underlying $L(0°)$ and $L(90°)$ have been averaged over 5° of azimuth (see Fig. 10). However, Fig. 11's polarization profile does show both a Babinet point and the reduced magnitude of p_Q in the optically thick clouds near the horizon.

In Fig. 3(b) we see p_Q at the same site almost 1 h earlier, only now the map is nearly perpendicular to the Sun's direction (at $\phi_{rel} = 104°$ here, $97° < \Psi < 104°$). As expected, p_Q is both large and positive in this part of the sky, increasing toward the left-hand side of the map (i.e., toward $\phi_{rel} = 90°$). As in Fig. 2(b), $p_Q \sim P$ here because the maximum-brightness $L(0°)$ image produced consistently large p_Q. Thin

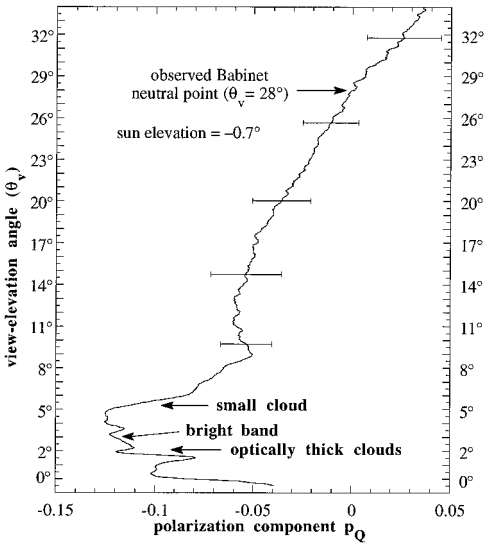

Fig. 11. Clear-sky p_Q ($\approx P$ here) near Marion Center, Pa., on 31 August 1996 at 2352 UTC for $\phi_{rel} = 0°$ [see Fig. 3(a)]. Each error bar spans two standard deviations of p_Q at the given θ_v and is calculated from the standard deviations of Fig. 10's radiances.

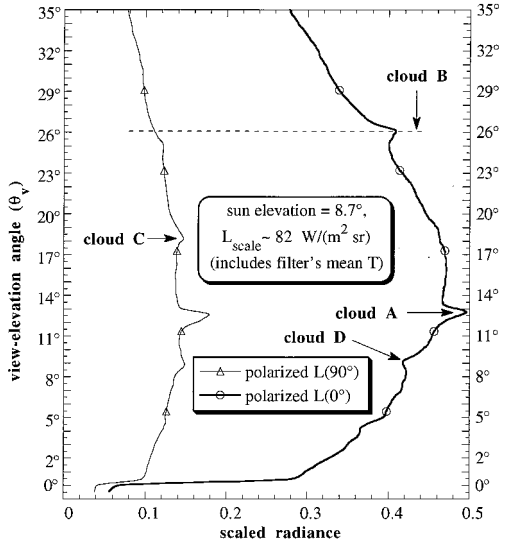

Fig. 12. Polarized clear-sky radiances near Marion Center, Pa., on 31 August 1996 at 2259 UTC. The Sun elevation = 8.7°, and $\phi_{rel} = 104°$. Radiances were averaged 2.5° on either side of $\phi_{rel} = 104°$, and the $L(0°)$ were measured at the filter orientation that produced the brightest image of this scene. Here small cumulus usually are brighter than their surroundings, with the notable exception of cloud D's $L(0°)$.

clouds near the horizon eliminate the strong p_Q gradients evident above Fig. 2(b)'s horizon. Several small cumulus appear near the horizon and the right-hand sides of Fig. 3(b)'s original photographs. These clouds usually are local minima of p_Q, and I have marked several of them with asterisks.

However, the two clouds labeled A and B in Fig. 3(b) are both local minima *and* maxima in the clear-sky p_Q field. All visible parts of these two clouds were sunlit, and the optical thickness of the air column between the camera and them could not have varied significantly over their small angular extents. This should rule out any differential airlight polarization between the clouds' tops and bottoms. The optical thicknesses of the clouds themselves do not appear very different in the $L(0°)$ and $L(90°)$ images. Given that $\Psi < 104°$, we are not near the cloudbow's polarization maximum. Thus we have no ready explanation for the unusual polarization patterns in clouds A and B, a puzzle complicated by the fact that other small cumulus nearby are consistently depolarized compared with the surrounding clear sky.

Note in Fig. 12 that θ_v of cloud B's local radiance maximum shifts ~1° between the $L(0°)$ and the $L(90°)$ images (cloud A's vertical shift is much smaller). In Fig. 13 we see the corresponding fluctuation in cloud B's p_Q values. Although Fig. 12 helps explain cloud B's polarization pattern mathematically, it provides no physical insight into the problem. And even if four-image polarization P eliminated cloud B's local polarization maximum, that would not explain why it exists for p_Q. As indicated by Fig. 3(b), all other clouds in Fig. 13 (including A for $\phi_{rel} = 104°$) appear only as depolarized areas in the clear-sky p_Q field. None of this complexity was evident during photography, when I saw the small cumulus merely as annoying contaminants of the clear sky. In retrospect these clouds pose Fig. 3(b)'s most interesting problem.

6. Simple Double-Scattering Model of Polarization

Numerous models of clear-sky polarization are extant,[10,11,45] so one adds to the list with caution. However, as a first-approximation comparison of observation and theory, my earlier model of clear-sky radiances has been extended to include p_Q (and P in

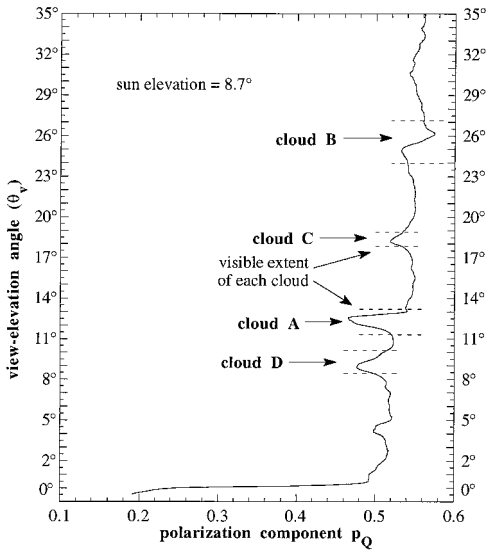

Fig. 13. Clear-sky p_Q ($\sim P$) near Marion Center, Pa., on 31 August 1996 at 2259 UTC for $\phi_{rel} = 104°$ [see Fig. 3(b)]. Although most small cumulus here are local p_Q minima, note that cloud B is both a local p_Q minimum and maximum.

the principal plane).[46] The extension consists of using phase functions for haze and molecular scattering that assume polarized rather than unpolarized incident light.[47] One then tracks the integrals of direct and diffuse skylight contributions along a specified slant optical path, with the final values of perpendicular- and parallel-polarized radiances at the observer determining p_Q. The model yields quite plausible patterns of p_Q, including a band of maximum polarization at $\Psi = 90°$ and neutral bands such as those seen in Figs. 2 and 3. Whatever its sins of incompleteness, this model has the virtue of being a straightforward double-scattering approximation to the radiative transfer equation.

However, my goal here is not to scrutinize the details of an admittedly preliminary model. Rather, I want to see whether it can begin to simulate the detailed p_Q observations discussed above. Because this simple double-scattering model cannot account for polarization asymmetries about the principal plane or those due to cloud scattering, I have not considered the Marion Center p_Q (see Fig. 3). However, by using the Deirmendjian haze-M aerosol-size distribution and varying the aerosol normal optical depth τ_a, the model has yielded good fits to the Chesapeake Beach p_Q profiles (see Figs. 6 and 9). At $\lambda = 475$ nm, the best fit is for a molecular normal optical depth of 0.15 and $\tau_a = 0.05$. In the antisolar case (Fig. 6), the model's predicted Arago neutral point is 1.7° lower than that observed, and the two polarization profiles have a rms difference of 0.0359 above the horizon. Near the horizon, however, the model's p_Q approaches -0.2, approximately twice the observed polarization.

The much better near-horizon agreement seen in Fig. 9, coupled with the fact that specularly reflected sunlight does not exist there, suggests that the model's Lambertian surface is a likely source of Fig. 6's errors. Figure 9's rms difference of 0.0309 is slightly smaller than Fig. 6's, with the largest differences occurring near the image's top, where the observed polarization decreases rapidly. A major failing of the model is that, for the given scattering geometry (i.e., solar elevation $= -0.46°$), it cannot produce p_Q maxima off the principal plane, contrary to what we see in Fig. 2(b). Possible solutions here include using a wider range of aerosol-scattering phase functions and examining the resulting Mueller matrices' effects.

Naturally, the comparisons of model and observations above are illustrative rather than definitive. Duplicating (or even approximating) the complex polarization patterns seen in Figs. 2 and 3 will require a much more sophisticated model. I am now developing a Monte Carlo model that will explicitly calculate Mueller matrix transformations of incidence Stokes parameters at each scattering. As with all Monte Carlo models, one can ultimately incorporate into it complex spatial distributions of scatterers and surface reflectance. The new model will simulate patterns of P that could be compared with fish-eye maps of clear-sky polarization. Yet even the present simple form of the double-scattering model offers a level of realism comparable with that found in other models (e.g., Ref. 1, pp. 215–217). As an instructive point of departure, it has considerable merit.

7. Two- and Four-Image Maps of Antisolar Clear-Sky Polarization

By how much do the two-image p_Q and the four-image P differ in a given scene? Figure 4 shows the complicated relationship between the two polarization parameters in one antisolar sky at sunset. The two maps are of the same clear sky photographed at the coastal site of Annapolis, Md., on 12 March 1997, when the Sun was 2.4° above the horizon. In Fig. 4(a) we see the familiar p_Q neutral band colored in red ($|p_Q| < 0.002$), which once again is asymmetric about the principal plane. As expected, negative p_Q lie below this band and positive p_Q above it. As points of reference, three distant radio towers near $\phi_{rel} = 180°$ form dotted red lines of neutral p_Q that extend from the neutral band to the horizon.

In contrast, Fig. 4(b)'s four-image map of P reduces the near-neutral band to a roughly circular area that straddles the principal plane. If we overlay the two maps, the near-neutral P region falls mostly within its p_Q counterpart. Although that overlap is expected, what is not is that the neutral band's lowest θ_v occurs at a different azimuth than does the P neutral area. Furthermore, P maps of other antisolar skies at sunset show circular Arago areas several degrees off the principal plane. Thus we have digital-image confirmation of Brewster's (and others') naked-eye observations of supposedly anomalous neutral points.[48] Finally, all of Fig. 4(b)'s P contours are slightly irregular, suggesting that asymmetries in p_Q maps are not artifacts of that technique.

Figure 14 shows P and $|p_Q|$ averaged over a 5°-wide azimuthal swath that is centered on $\phi_{rel} = 180°$ in Fig. 4. As above, P and $|p_Q|$ are essentially the same in the principal plane, even though their averages include polarization data from just outside it. In fact, the largest difference between P and $|p_Q|$ occurs near the p_Q Arago point at $\theta_v = 9.3°$. Whatever the higher P values' physical explanation is there, their mathematical explanation is clear enough. As expected in the principal plane, the average U is much smaller than the average Q (~4.6 times smaller). Both Q and U change sign near $\theta_v = 9.3°$, although U is negative only briefly. However, the zeros of Q and U occur at different θ_v, meaning that their sum in Eq. (2) is never zero. Thus, although the four-image P is very small near p_Q's Arago point, that average P is never identically zero, even if we smooth over a narrower azimuthal swath. However, when we consider individual pixels in Fig. 4(b), rather than azimuthal averages, then neutral and near-neutral P values abound.

Note that the four-image technique produces an inherently smoother map than the two-image technique. Some of this smoothing stems from the fact that four pixels, rather than two, are added to form Eq. (2)'s normalizing term I. Other smoothing is

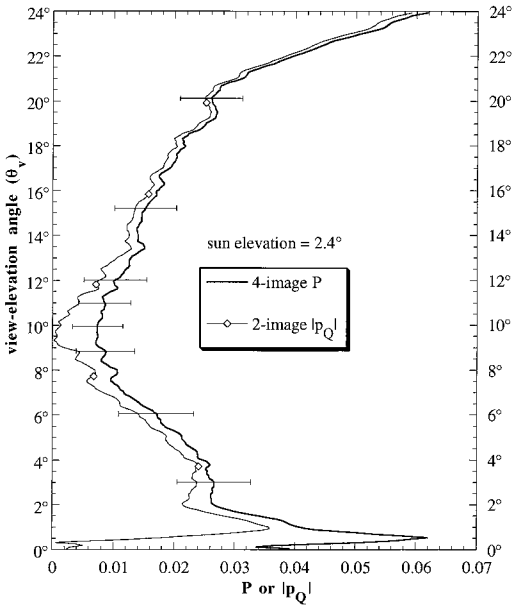

Fig. 14. Clear-sky polarization P and its component $|p_Q|$ at Annapolis, Md., on 12 March 1997 at 2255 UTC for $\phi_{rel} = 180°$ (see Fig. 4). Both P and p_Q were averaged 2.5° on either side of the principal plane. Each error bar spans two standard deviations of P at the given θ_v. Topography that extends slightly above the astronomical horizon produces the large variations in P and $|p_Q|$ below $\theta_v = 2°$.

due simply to the four-image technique's larger pixel registration errors. This four-image smoothing and its resulting polarization reductions are evident in Fig. 4(b), in which red pixels have all but disappeared below the horizon and in the radio towers. Less near-neutral polarization appears in Fig. 4(b), despite the fact that its threshold for red pixels has been increased to $P < 0.005$. For 24-bit images, this larger P threshold represents a difference of only one or two gray levels in each color channel of the original digital images. Thus we still are close to the threshold of quantization errors. In any event, reducing the neutral P threshold to 0.002 (or even 0.0) simply yields fewer red pixels in the sky, not just one.

Thus even our highest-resolution analysis of P will not replace Fig. 4(b)'s near-neutral area with a single Arago neutral point. This should not alarm us any more than the knowledge that a pressure minimum on a weather map corresponds to an area, rather than a point, of lowest pressure. Although it is convenient to think of neutral points (or even neutral lines), we should not be surprised that the real atmosphere is more complicated than our mental (and computer) models of it. Similarly, we should not assume that neutral P outside the principal plane is somehow an anomaly. The atmosphere is a template for our models, not the reverse.

8. Conclusions

Digital-image analysis can transform clear-sky photographs into a rich and reliable source of polarization data. This new data source not only has very high angular and temporal resolutions, but it also lets us see polarization patterns over large areas (e.g., Figs. 2–4). These maps provide several new insights. First, as expected, the polarization parameters P and p_Q do have different spatial patterns in the clear sky, but clearly these are related to each other. As Dorno's extensive measurements of Q suggest, p_Q is a useful polarization measure. Yet, because it is based on less information than P, p_Q requires especially careful interpretation. Second, regardless of whether we use P or p_Q, the Arago neutral point (and presumably others) has many neutral and near-neutral neighbors. The term neutral point is perfectly acceptable so long as we remember that skylight polarization actually will be indistinguishably different from zero in an area around our chosen neutral point. Third, multiple scattering will create strong p_Q and P gradients in the near-horizon sky at right angles from a low Sun. These gradients are diminished if skylight at higher θ_v is also dominated by multiple scattering (i.e., if it is weakly polarized). With hindsight, this observation may seem almost self-evident, yet Fig. 2(b) provides the first unambiguous confirmation of the gradients' existence. Fourth, maps of both P and p_Q indicate that skylight polarization (and radiance) probably should be assumed to be asymmetric, rather than symmetric, about the principal plane. As convenient as the latter assumption is, it should not automatically constrain skylight models.

Of course, we need not fret about whether a model can duplicate every irregularity observed in a given clear-sky polarization map. More important is that skylight models now have a new, and much more detailed, standard for verisimilitude, one derived from digital imaging of clear-sky polarization.

This research was supported by U.S. National Science Foundation grant ATM-9414290. Additional funding came from the Commander, Naval Meteorology and Oceanography Command. I am indebted to Günther Können and Kenneth Voss for their perceptive comments during the course of this research. Jacob Foret provided additional insights and ably assisted me in taking Fig. 4's original photographs.

References and Notes

1. K. L. Coulson, *Polarization and Intensity of Light in the Atmosphere* (Deepak, Hampton, Va., 1988), pp. 375–391.
2. J. W. Strutt, "On the light from the sky, its polarization and colour," Philos. Mag. **41,** 107–120, 274–279 (1871).
3. Reference 1, pp. 269–270, lists skylight polarization studies by several of Rayleigh's contemporaries.
4. S. Chandrasekhar and D. Elbert, "The illumination and polarization of the sunlit sky on Rayleigh scattering," Trans. Am. Philos. Soc. **44,** Pt. 6, 643–728 (1954).
5. H. Neuberger, *Introduction to Physical Meteorology*, Revised ed. (Pennsylvania State University, University Park, Pa., 1957), pp. 194–206.
6. Z. Sekera, "Light scattering in the atmosphere and the polarization of sky light," J. Opt. Soc. Am. **47,** 484–490 (1957).
7. K. L. Coulson, "Effects of the El Chichon volcanic cloud in the stratosphere on the polarization of light from the sky," Appl. Opt. **22,** 1036–1050 (1983).

8. F. E. Volz, "Volcanic turbidity, skylight scattering functions, sky polarization, and twilights in New England during 1983," Appl. Opt. **23,** 2589–2593 (1984).
9. See Ref. 1, pp. 377–378.
10. E. de Bary, "Influence of multiple scattering of the intensity and polarization of diffuse sky radiation," Appl. Opt. **3,** 1293–1303 (1964). The atmospheric principal plane is also called the Sun's vertical.
11. R. S. Fraser, "Atmospheric neutral points outside of the principal plane," Contrib. Atmos. Phys. **54,** 286–297 (1981).
12. K. Bullrich, "Scattered radiation in the atmosphere and the natural aerosol," Adv. Geophys. **10,** 99–260 (1964). Polarization measurements that span half of the sky dome appear on pp. 212–215 (Figs. 49 and 50). Also see Ref. 1, pp. 216–218, 311, 325, 327.
13. T. Prosch, D. Hennings, and E. Raschke, "Video polarimetry: a new imaging technique in atmospheric science," Appl. Opt. **22,** 1360–1363 (1983). Also see Ref. 1, p. 554.
14. E. J. McCartney, *Optics of the Atmosphere: Scattering by Molecules and Particles* (Wiley, New York, 1976), pp. 213, 268.
15. D. J. Gambling and B. Billard, "A study of the polarization of skylight," Aust. J. Phys. **20,** 675–681 (1967).
16. F. S. Harris, Jr., "Calculated Mie scattering properties in the visible and infrared of measured Los Angeles aerosol size distributions," Appl. Opt. **11,** 2697–2705 (1972).
17. For examples, see Ref. 1, pp. 256–261.
18. Ref. 5, p. 197.
19. Ref. 1, p. 233. Also see E. Collett, *Polarized Light: Fundamentals and Applications* (Marcel Dekker, New York, 1993), pp. 34–39.
20. C. F. Bohren and D. R. Huffman, *Absorption and Scattering of Light by Small Particles* (Wiley, New York, 1983), pp. 50–53.
21. Ref. 20, p. 53.
22. B. W. Fitch, R. L. Walraven, and D. E. Bradley, "Polarization of light reflected from grain crops during the heading growth stage," Remote Sensing Environ. **15,** 263–268 (1984).
23. See Ref. 1, p. 254 and Ref. 20, p. 50.
24. Ref. 20, pp. 46, 50. χ has the same direction as skylight's plane of polarization but avoids the conceptual difficulties that a plane of (partial) polarization entails.
25. For examples, see Ref. 1, pp. 554–555 and 565–566.
26. For example, see Ref. 5, pp. 194–197. Lines of zero Q are still called neutral lines (Ref. 1, pp. 254–258).
27. ϕ_{rel} ranges between 0° and 360°, with values increasing clockwise from the Sun's azimuth.
28. Ref. 1, p. 254.
29. Ref. 20, pp. 382–383. Equation (4) also defines polarization for specular reflection from planar surfaces. χ is horizontal for linear polarization by reflection from horizontal surfaces (e.g., calm water). To measure this polarization, once again set Eq. (4)'s 0° direction parallel to χ (i.e., horizontal).
30. Ref. 20, p. 54.
31. Ref. 14, pp. 198–199.
32. Ref. 14, pp. 136–139. Note that 475 nm is a dominant wavelength typical of clear skies.
33. R. L. Lee, Jr., "Colorimetric calibration of a video digitizing system: algorithm and applications," Color Res. Appl. **13,** 180–186 (1988).
34. For a remote-sensing application of P derived from photographs, see K. L. Coulson, V. S. Whitehead, and C. Campbell, "Polarized views of the earth from orbital altitude," in *Ocean Optics VIII*, M. A. Blizard, ed., Proc. SPIE **637,** 35–41 (1986). Narrow-FOV photographic polarimetry that uses a Savart plate is discussed in R. Gerharz, "Polarization of scattered horizon light in inclement weather," Arch. Meteorol. Geophys. Bioklimatol. Ser. A **26,** 265–273 (1977).
35. For example, see Ref. 1, p. 261 (Fig. 4.36). θ_v is 0° at the astronomical horizon, except in Figs. 10–13, where θ_v is 0° at the slightly higher mean topographic horizon (see Fig. 3).
36. My polarizer's H_{90} is fairly uniform at visible wavelengths, although crossed pairs of such polarizers do transmit a dim violet from a white-light source. Because skylight dominant wavelengths at the Earth's surface typically are 475 nm or more, the increase in photographic polarizers' H_{90} at shorter wavelengths is unlikely to appreciably bias observations of skylight polarization.
37. See Ref. 1, p. 582, for the general form of these Mueller matrix calculations.
38. As noted above, P measured by the four-image technique depends only on a polarizer's relative (rather than absolute) directions of 0°, 45°, 90°, and 135°. In other words, the four-image 0° direction can differ arbitrarily from χ.
39. R. Gerharz, "Self polarization in refractive systems," Optik **43,** 471–485 (1975). Coulson calls self-polarization parasitic polarization (Ref. 1, p. 556).
40. See Ref. 1, pp. 254–258.
41. R. S. Fraser, "Atmospheric neutral points over water," J. Opt. Soc. Am. **58,** 1029–1031 (1968). Also see Ref. 1, pp. 381–382.
42. See Ref. 1, pp. 522–525, for a discussion of partial polarization on reflection by water.
43. Ref. 1, p. 311 (Fig. 5.22). Large near-horizon p_Q gradients at 90° from a low Sun appear consistently in my polarization maps.
44. Usually red pixels in Figs. 2–4 are the result of identical 24-bit colors in the original digital images; so, in a limited sense, the maps do include points where p_Q and $P = 0.0$ exactly, but this equality is just an artifact of the resolution with which the slide scanner quantized scene radiances.
45. For example, K. F. Evans and G. L. Stephens, "A new polarized atmospheric radiative transfer model," J. Quant. Spectrosc. Radiat. Transfer **46,** 413–423 (1991).
46. R. L. Lee, Jr., "Horizon brightness revisited: measurements and a model of clear-sky radiances," Appl. Opt. **33,** 4620–4628, 4959 (1994).
47. Ref. 20, pp. 112–113.
48. Ref. 1, pp. 391–393.